# NOTICE

## CERTAIN DATA CONTAINED IN THIS DOCUMENT MAY BE DIFFICULT TO READ IN MICROFICHE PRODUCTS.

Conf-920804--15

ANL/CP--76052

DE92 016601

# The Influence of the Prandtl Number on the Thermal Performance of Tubes With the Separation and Reattachment Enhancement Mechanism

T. J. Rabas and B. Arman

Energy Systems Division
Argonne National Laboratory
9700 S. Cass Avenue
Argonne, IL 60439

JUL 3 1992

## ABSTRACT

This paper demonstrates that the heat-transfer performance of an enhanced tube with transverse, rectangular disruptions can be predicted with a numerical modeling method, an accompiishment not previousiy achieved. This computer code is then used to determine the influence of the Prandtl number. The numerical simulation demonstrated that six distinct regions exist: the three rib surfaces, the upstream and downstream recirculation regions, and the boundary-layer development zone. Three zones dominate the thermal performance: the rib top and downstream faces and the downstream recirculation zone. The thermal performance at the rib region begins to dominate the overall performance as the Prandtl number becomes large. The contribution from the downstream recirculation zone becomes more important and dominates for low Prandtl number fluids such as air. The Reynolds number dependence at the rib region and the downstream recirculation zone is similar to that for reattaching flows with exponents in the 0.65 to 0.75 range. The location of the maximum in the recirculation moves closer to the rib with increasing Reynolds and Prandtl numbers and is bounded upstream by the location of the maximum wall shear stress and downstream by the reattachment length. The high turbulence level near the surface in this region is responsible for the heat-transfer enhancement.

## NOMENCLATURE

| | |
|---|---|
| $A_\varepsilon$ | constant in dissipation length scale |
| $A_\mu$ | constant in viscosity length scale |
| B | logarithmic-law constant |
| $c_l$ | a constant in length scale equations |
| $c_p$ | specific heat |
| $c_\mu$ | turbulence model constant |
| $d_i$ | tube diameter |
| e | rib height |
| $e_{sg}$ | equivalent sand-grain roughness height |
| $e^+$ | roughness Reynolds number, $e^+ = (e/d_i)u_\tau/\nu$ |
| $e_{eg}^+$ | sand-grain roughness Reynolds number, $e_{eg}^+ = (e_{sg}/d_i)u_\tau/\nu$ |
| f | friction factor |
| $f_p$ | plain-tube friction factor |
| k | turbulent kinetic energy |
| $l_\varepsilon$ | dissipation length scale |
| $l_\mu$ | eddy viscosity length scale |
| m | Prandtl number exponent |
| n | Reynolds number exponent |
| Nu | Nusselt number |
| $Nu_p$ | plain-tube Nusselt number |
| p | pressure |
| $p$ | disruption or rib pitch |
| Pr | Prandtl number |
| r | radial distance |
| Q | total heat added per pitch |
| Re | Reynolds number based on tube diameter, $Re = \rho d_i U/\mu$ |
| $R_y$ | Turbulent Reynolds number, $R_y = yk^{1/2}/\nu$ |
| St | Stanton number |
| $St_p$ | plain-tube Stanton number |
| T | temperature |
| u | axial velocity |
| U | average velocity |
| $u^+$ | nondimensional velocity, $u^+ = u/u_\tau$ |
| $u_\tau$ | friction velocity, $u_\tau = \sqrt{\tau_w/\rho}$ |
| v | radial velocity |
| w | disruption width |
| W | total mass flux |
| x | axial distance |
| y | normal distance from the wall |
| $y^+$ | wall coordinate, $y^+ = yu_\tau/\nu$ |

### Greek Letters

| | |
|---|---|
| $\varepsilon$ | turbulent energy dissipation |
| $\kappa$ | Karman constant |
| $\mu$ | viscosity |
| $\nu$ | diffusivity |
| $\rho$ | density |
| $\eta$ | efficiency index, $\eta = (St/St_p)/(f/f_p)$ |
| $\tau_w$ | wall shear stress |
| $\Delta p$ | pressure drop |
| $\Delta T$ | temperature rise |

Work supported by the U.S. Department of Energy, Assistant Secretary for Conservation and Renewable Energy, Office of Industrial Technology, Advanced Industrial Programs, under contract W-31-109-Eng-38.

MASTER

DISTRIBUTION OF THIS DOCUMENT IS UNLIMITED

## DISCLAIMER

This report was prepared as an account of work sponsored by an agency of the United States Government. Neither the United States Government nor any agency thereof, nor any of their employees, makes any warranty, express or implied, or assumes any legal liability or responsibility for the accuracy, completeness, or usefulness of any information, apparatus, product, or process disclosed, or represents that its use would not infringe privately owned rights. Reference herein to any specific commercial product, process, or service by trade name, trademark, manufacturer, or otherwise does not necessarily constitute or imply its endorsement, recommendation, or favoring by the United States Government or any agency thereof. The views and opinions of authors expressed herein do not necessarily state or reflect those of the United States Government or any agency thereof.

## INTRODUCTION

Perhaps one of the least understood aspects of single-phase enhanced surfaces is the influence of the Prandtl number, Pr. The quantity of experimental data available to explore the influence of the Prandtl number is limited and only a few publications address its importance. As a result, the heat-exchanger designer does not have access to high-quality prediction methods and must depend on experimental data using fluids of interest to select the best enhanced-tube geometry for each particular application.

### Enhancement Geometry

This paper explores the impact of the Prandtl number on the thermal performance for a very important category of enhanced tubes. These tubes contain disruptions which are nearly transverse to the flow direction and with a spacing greater than the reattachment length. This geometry was proposed and/or used for many single-phase forced convection applications, and falls into a mechanism category called separation and reattachment (Rabas, 1989). Figure 1 shows the separation regions and the flow reattachment that occurs between the disruptions with this essentially two-dimensional flow field. A square disruption shape is shown; however, contoured disruption shapes exist with commercially available heat-exchanger tubes.

### Experimental Results

There are a number of experimental investigations that obtained heat-transfer data for a range of Prandtl numbers but for enhancement mechanisms other than the separation and reattachment. Using three-dimensional, internally roughened passages (the boundary-layer thinning mechanism), heat-transfer data were obtained by Dipprey and Sabersky (1963) and Gowen and Smith (1968) with water at different temperature levels. Also, using three-dimensional roughness surfaces, mass-transfer data were obtained by Dawson and Trass (1972) with Schmidt numbers varying from 1000 to 7000. Using an internally threaded pipe (the separation and recirculation mechanism), Smith and Gowen (1965) compared the thermal performance obtained with water and Ucon (a polyalkylene glycol, Pr = 349). Carnavos (1980, 1979) obtained experimental heat-transfer data using internally finned tubes (the extended-surface enhancement mechanism) for both air and water. No further reference will be made to these publications because they present data for mechanisms other than separation and reattachment.

Burck (1970), being aware of the importance of the Prandtl number, presented a very comprehensive evaluation of the existing data at that time although he did not make a distinction between the various enhancement mechanisms. He concluded that influence of the Prandtl can be displayed with the efficiency index, $\eta = (St/St_p)/(f/f_p)$, as a function of the equivalent sand-grain roughness Reynolds number, $e^+_{sg}$, as shown in Figure 2. Note that the efficiency index increases with the Prandtl number and values greater than unity can only be obtained with the higher Pr fluids.

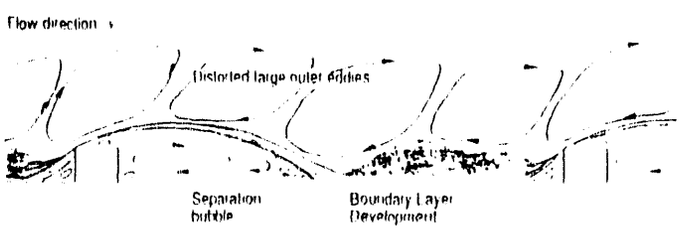


FIGURE 1 Schematic of the Turbulent Flow Structure Within an Enhanced Tube with the Separation and Reattachment Mechanism

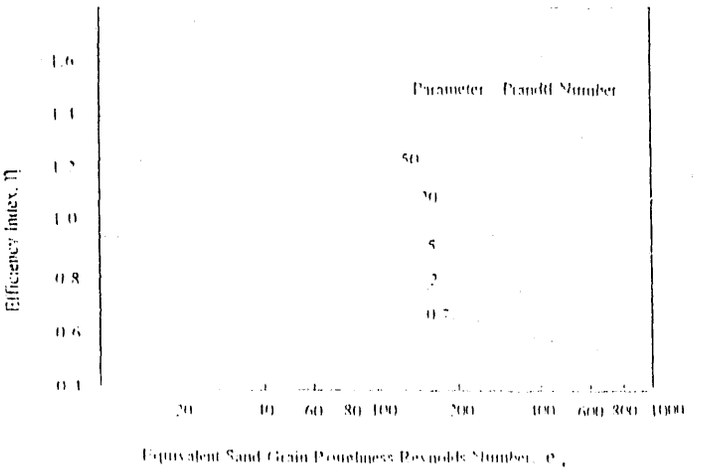


FIGURE 2 Efficiency-Index Variation with the Equivalent Sand-Grain Roughness Reynolds Number Developed by Burck (1970)

Burck stated that this curve could be used to calculate the heat transfer for all types of enhanced surfaces if the friction factor and the Prandtl number are known. The majority of the data used to develop this figure was obtained with closed-spaced triangular grooves (his data) and that of Dipprey and Sabersky (1963). It is shown in the Appendix that there are substantial errors between this prediction method and the data of Webb et al. (1971) to be discussed.

There are five publications that presented heat- or mass-transfer data for a range of Prandtl numbers taken with enhancement tube geometry characteristic of the separation and reattachment mechanism.

**Savage and Myers (1963).** Savage and Myers (1963) conducted heat-transfer and pressure-drop experiments with rectangular disruptions in a circular pipe with water as the test fluid. The water temperature was varied to investigate the Prandtl number effect for a limited range ($2 < Pr < 8$). The heat-transfer experiments were conducted with only a single disruption being thermally active. As a result, the water approached the heated disruption with a uniform rather than a non-uniform temperature distribution; the latter, of course, would exist if the upstream disruptions were thermally active. Because of only the local heating, the authors stated that their heat-transfer data are of limited value for predicting the thermal performance when heating occurs for the entire tube length.

**Kalinin et al. (1970).** An extensive analysis of the heat-transfer and pressure-drop performance of transverse, grooved tubes was conducted in the USSR in the 1960s and summarized by Kalinin et al. (1970). Most of the data were taken with air as the test fluid but a limited number of water data appears to have been taken although not presented in the paper. Correlations were presented in the form $Nu/Nu_s = f(Re, e/d_i, p/e)$ with no Prandtl number correction. It will be shown that this finding is not in agreement with the other data to be discussed. A possible explanation is that only limited water data were available for this correlation effort.

**Webb et al. (1971).** Webb et al. (1971) presented data obtained for a broad Prandtl number range with an enhanced tube geometries characteristic of the separation and reattachment mechanism. They used four different fluids (air - Pr = 0.71, water - Pr = 5.1, n-butyl alcohol - Pr = 21.7, and butyl alcohol - Pr = 37.6) in their benchmark experiments. Five different tube geometries with transverse, rectangular disruptions or ribs were tested (see Table 1).

Table 1 - Tube Geometries Tested by Webb et al. (1971) with D = 36.8 mm (1.45 in)

| Tube No. | e/D | p/e | w/e |
|---|---|---|---|
| 01/10 | 0.01 | 10 | 1.034 |
| 02/10 | 0.02 | 10 | 0.517 |
| 04/10 | 0.04 | 10 | 0.259 |
| 02/20 | 0.02 | 20 | 0.517 |
| 02/40 | 0.02 | 40 | 0.517 |

Figure 3 shows the measured heat-transfer enhancement values plotted as a function of the roughness Reynolds number with the Prandtl number as a parameter for the 01/10 tube shown in Table 1. There is a very pronounced maximum enhancement level and the level increases as the Prandtl number increases. The maximum occurs at a lower $e^+$ and the $e^+$ range decreases as the Prandtl number increases. Curves of the data for the other tubes are very similar in shape with the major difference being the locations and the magnitude of the enhancement levels. This characteristic of the enhancement level suggests a geometry-selection procedure based on the roughness Reynolds number as described by Webb (1979). However, there is no satisfactory explanation why the Prandtl number had this effect on the enhancement level.

Figures 4 and 5 present the Reynolds number and Prandtl number exponents with the Reynolds number as a parameter for the 04/10 and 01/10 tubes, respectively. These exponents were obtained from second-order polynomial curve fits of the experimental data in the form ln (Nu) with ln (Re) for fixed Pr, and ln (Nu) with ln (Pr) for fixed Re. Also shown in these figures are the n and m values for a plain tube based on the commonly used Petukhov and Popov correlation (Petukhov, 1970). Both figures show that the variations of the exponents for the two enhanced tubes are very different from a plain tube and also from each other. For the smooth tubes and for a fixed Prandtl number, both m and n increase with the Reynolds

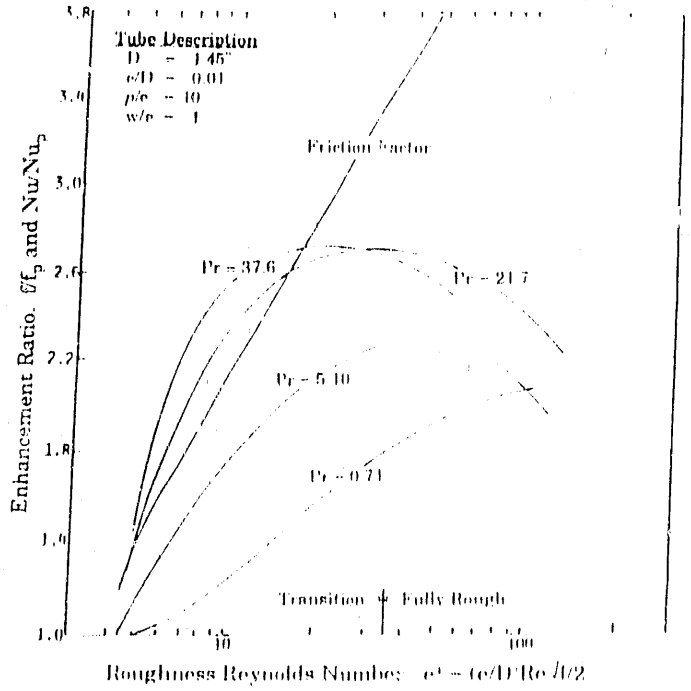


FIGURE 3 Heat Transfer Enhancement as a Function of the Roughness Reynolds Number Based on the Data of Webb et al. (1971)

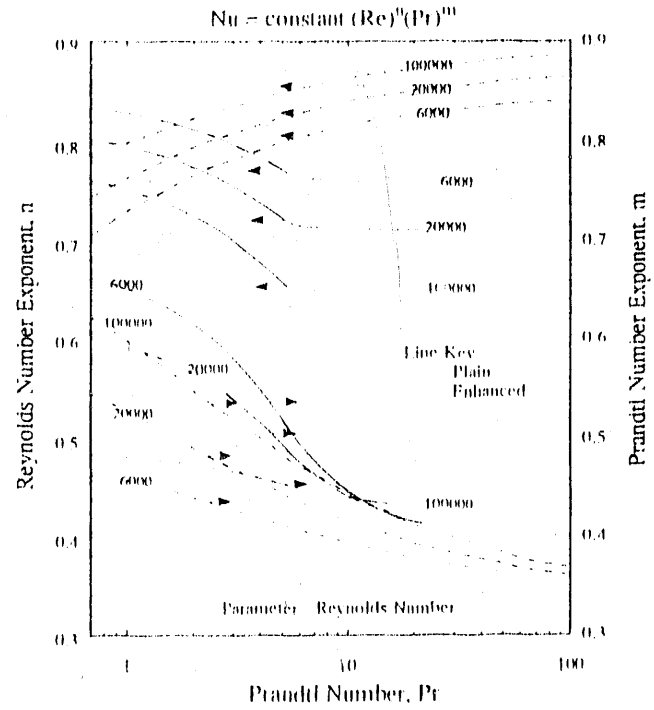


FIGURE 4 Reynolds and Prandtl Number Exponents as a Function of the Prandtl for the 04/10 Tube Geometry Tested by Webb et al. (1971)

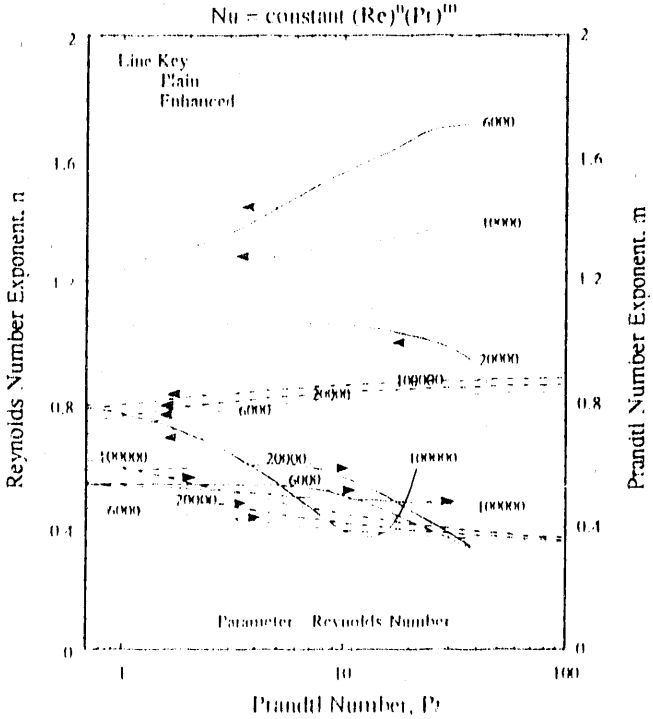


FIGURE 5 Reynolds and Prandtl Number Exponents as a Function of the Prandtl for the 01/10 Tube Geometry Tested by Webb et al. (1971)

number. For the enhanced tubes, almost the exact opposite is obtained, the only exception being the Prandtl number exponent at Pr greater than about 10. The magnitude of the Prandtl number exponents for the two enhanced tubes and the smooth

tube are not too different; they essentially decrease with an increase of the Prandtl number and are bounded by about 0.65 for Pr = 0.7 to about 0.35 for very large Pr values.

The most dramatic variation is with the Reynolds number exponents, especially for the 01/10 tube geometry. Note that the exponent changes from increasing to decreasing with a fixed Pr as the Reynolds number increases. For the lower Re values, there is a significant thermal-performance improvement with increasing Prandtl number; however, this improvement occurs with the 01/10 tube at low Re values but not for the 04/10 tube. For the 04/10 tube, there is a general decrease of n with Pr and it appears to reach different asymptotic values which are a function of the Re value. For the larger Re values, n is in the 0.65 to 0.72 range. The magnitude of n for the larger disruption or rib and the largest Reynolds number range is an important finding that will be discussed later. In addition, the sometimes used Wilson plot method for data reduction can be questioned because the heat-transfer coefficient is assumed to have a fixed-exponent dependence on the velocity or Reynolds number.

**Berger and Hau (1979).** Berger and Hau (1979) used the electrochemical analogue technique to measure the local and mean mass-transfer performance in a pipe with transverse, square disruptions with a height to diameter ratio of 0.036 and with different pitch to height ratios. The Schmidt number varied over a wide range from 1000 to 7000. The major findings for the 036/10 tube were as follows:

1) The Prandtl number exponent did not vary from a value of about 0.33.

2) The exponent on the Reynolds was 0.695, which is substantially lower than that obtained with smooth-tube prediction methods (about 0.85) for high Pr fluids.

3) The variations between the maximum and minimum local mass-transfer values and the mean value decreased with increasing Reynolds number; in other words, the mass-transfer distribution became more uniform. The maximum values are located at the top of the rib and near the reattachment point and the minimum values are located directly in front and behind the rib.

4) The point of maximum heat transfer moves closer to the rib as the Reynolds number increases.

The first two observations for the 036/10 tube are consistent with the data of Webb et al. (1971) for the 04/10 tube shown in Figure 4. The local data, which were used to obtain the last two observations, are useful in obtaining a fundamental understanding of how the Prandtl number influences the performance; unfortunately, they were obtained with large Schmidt number values.

**Tan and Xaio (1989).** Figure 6, presented by Tan and Xaio (1989), also shows the enhancement levels as a function of the roughness Reynolds number with the Prandtl number as a parameter. These results are for a tube with a contoured disruption shape. The tube is the single-start, spirally indented type with e/d$_i$ and *p*/e values of approximately 0.053 and 10.8, respectively. The indenting process produces internal disruptions that are rounded or contoured without any sharp corners. Note the similarity between these data and those obtained by Webb et al. (1971) shown in Figure 3. For air (Pr = 0.7), the enhancement level increases with $e^+$ until a maximum is obtained. For liquids (Pr > 1), a maximum enhancement level is obtained; however, the maximum occurs at smaller $e^+$ values ($e^+ \approx 20$) and is less Prandtl number dependent than obtained for rectangular disruptions or ribs.

The experimental data shown in Figures 3 and 6 clearly

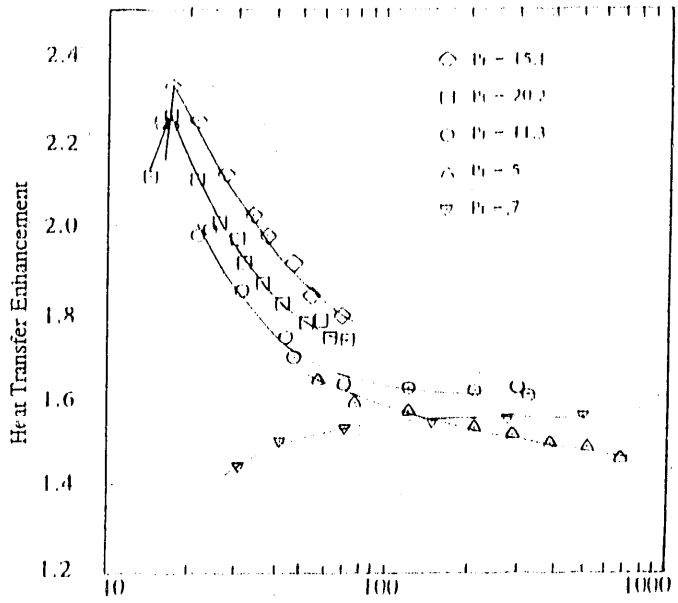


FIGURE 6 Enhancement Level Variation as a Function of the Roughness Reynolds Number Based on the Data of Tan and Xaio (1989)

demonstrate that the Prandtl number has an important impact on the performance of enhanced tubes with geometries characteristic of the separation and reattachment mechanism. In addition, the correlation recommended by Kalinin et al. (1970) that does not include the Prandtl number certainly cannot be correct.

The purpose of this paper is to explain this Prandtl number effect. The local heat-transfer performance was considered as essential to obtain this fundamental understanding. Experimental techniques such as the transient liquid-crystal method (Baughn and Yan, 1991) or the naphthalene-sublimation method (Mendes and Mauricio, 1987) are effective methods currently for just a single Prandtl number. Electrochemical analogue technique (Berger and Hau, 1979) is effective for a range of Schmidt numbers ($1000 < Sc < 7000$) but this range far exceeds the Prandtl number values for all commonly used fluids in heat-exchange applications. As a result, a numerical modeling approach was selected to explore this Prandtl number effect.

A brief description of the turbulence model, the numerical method, and comparisons with experimental results are presented next. The last part will explain how the Prandtl number influences the thermal performance.

## TURBULENCE MODEL, NUMERICAL METHOD, AND COMPARISONS

This section of the paper briefly describes the modeling approach that was selected; however, a detailed description is given by Arman and Rabas (1992). The same modeling approach (Arman and Rabas, 1991) was successfully used to predict the friction-factor variation with the Reynolds number for the tube geometries shown in Table 1. Additional refinements have recently been made that further improved the prediction accuracy and are discussed in detail by Arman and Rabas (1992).

The governing conservation laws supply the continuity

equation, the momentum equations, and the energy equation. The transport equations for k and ε are used for closure of the equation set. These governing equations are presented in many publications and therefore are not repeated here. The conservation equations coupled with the k-ε equations are the common starting point for almost all the current engineering numerical modeling efforts. The turbulence model employed is a two-layer turbulence model which is briefly described below.

## Two-Layer Turbulence Model

The two-layer model of Chen and Patel (1988) divides the flow domain into two regions: (1) a near-wall region that includes the sublayer, the buffer layer, and a small part of the turbulent core, and (2) the remainder of the fully developed turbulent core region. The standard k-ε model is used in the core region while a one-equation model is used in the near-wall region. The advantages of the near-wall one-equation model are that the turbulent kinetic-energy equation is solved in the near-wall region and that the near-wall treatment is dependent on the local turbulence intensity and not the wall shear stress.

The energy dissipation in the near-wall region is specified by

$$\varepsilon = k^{2/3}/l_\varepsilon$$

where the eddy viscosity is obtained from

$$\mu_t = c_\mu k^{1/2} l_\mu \quad ,$$

The length scales, $l_\mu$ and $l_\varepsilon$, contain the necessary damping effects in the near-wall region or

$$l_\mu = c_l y[1 - \exp(-R_y/A_\mu)]$$

$$l_\varepsilon = c_l y[1 - \exp(-R_y/A_\varepsilon)]$$

$$R_y = yk^{1/2}\rho/\mu$$

Note that both $l_\varepsilon$ and $l_\mu$ become linear and approach $c_l y$ with increasing distance from the wall. $c_l$ is given by

$$c_l = \kappa/c_\mu^{3/4}$$

to ensure a smooth eddy-viscosity distribution at the junction of the near-wall and fully-turbulent core region. In addition, $A_\varepsilon = 2c_l$ or is assigned a value to recover the proper asymptotic behavior of the kinetic energy in the sublayer

$$\varepsilon = 2\nu k/y^2$$

The parameter $A_\mu = 70$ is determined from numerical results to recover the additive constant, $B = 5.45$, in velocity log law for the case of a near-wall boundary-layer flow field. The $\kappa$ and $c_\mu$ constants are equal to 0.418 and 0.09, respectively.

The wall shear stress does not appear in this formulation and, in particular, in the turbulent Reynolds number, $R_y$. $R_y$ varies slowly along lines parallel to the wall, does not vanish at the separation point, and remains well-defined in the regions of the flow reversal. As a result, damping effects decay rapidly with the distance from the wall regardless of the magnitude of the wall shear stress.

The matching between the one-equation near-wall treatment and the two-equation standard k-ε model in the two-layer approach can be carried out along pre-selected grid lines, even for complex flows with separation. For this application, the match boundary was selected along a grid line with $y^+$ values in the range of 100 to 200, which is far from the near-wall region to ensure a smooth eddy-viscosity distribution across the boundary of the two regions.

## Numerical Method

The numerical method used for this study is the finite-volume method based on the algorithm of Patankar and Spalding (1972) that solves the steady, two-dimensional axisymmetric, incompressible conservation equations for the velocity variables, u and v, and for the scalar variables p, k, and ε. The scalar variables are computed and stored at the main grid locations while the velocity variables are computed and stored in their respective staggered locations.

The momentum, energy, turbulence kinetic energy, and dissipation transport equations are discretized using the finite-volume approach. The diffusive terms are discretized by second-order central differencing while the convective terms are discretized by two different schemes: (1) hybrid upwind, first-order central scheme (see Patankar, 1980) and (2) quadratic-upstream scheme (QUICK) of Leonard (1979) (also see Phillips and Schmidt, 1985). Most of the initial runs were made by the hybrid scheme due to its stability and good convergence behavior. The QUICK scheme was used to obtain the final results.

The velocity-pressure coupling is achieved through the use of the continuity equation applying the SIMPLEC algorithm (Van Doormaal and Raithby, 1984). The resulting algebraic equations were solved by using a line-by-line, three-diagonal matrix algorithm that sweeps in both directions.

The boundary conditions at the wall are the usual no-slip conditions; i.e, $u = v = k = 0$. There is no need to specify the wall boundary condition for ε. The wall boundary condition for the temperature is a constant wall heat flux. The axisymmetry conditions are used for the symmetry axis.

Periodicity conditions are used at the inlet and the outlet of the flow domain in order to represent a fully developed flow field. The domain length is equal to one rib pitch. Fully developed flow requires identical inlet and outlet profiles for the velocities, turbulent kinetic energy, and turbulent energy dissipation. The driving force for the flow is a constant pressure difference that exists between the inlet and outlet pressure distributions. As with the pressure profiles, the temperature profiles must be identical at the axial increments of one pitch except for a constant value displaced by an amount of $\Delta T = Q/Wc_p$. For more information on the periodicity boundary conditions and the fully developed flow constraint see Patankar et al. (1977).

The first near-wall grid point is located well within the laminar sublayer ($y^+ \sim 0.1$) for all of the iterations. The number of non-uniform r-grids and non-uniform x-grids were always larger than 50. The iteration dependency tests were performed and the iterations were continued until the normalized mass residual (total mass residuals divided by the total mass flow rate) fell below $10^{-5}$. The number of iterations ranged between 3000 - 7000; however, the required number of iterations for the temperature field were much larger (between 8000 - 15000).

## Comparisons with Experimental Results

The data of Webb et al. (1971) are used for these comparisons. Figure 7 presents a comparison of the measured and predicted Nusselt numbers as a function of the Reynolds number for different Prandtl numbers. The particular geometry selected for this comparison is the 02/20 tube (see Table 1). Note the very favorable agreement.

Table 2 presents a comparison of the measured data obtained by Webb et al. (1971) and the numerical predictions for the five tubes and four Prandtl numbers considered in their research. Note the good agreement with an average error of only 15 percent. In general, the numerical method underpredicts the experimental results with maximum errors occurring at the high Re range but never exceeding about 31 percent. Very favorable

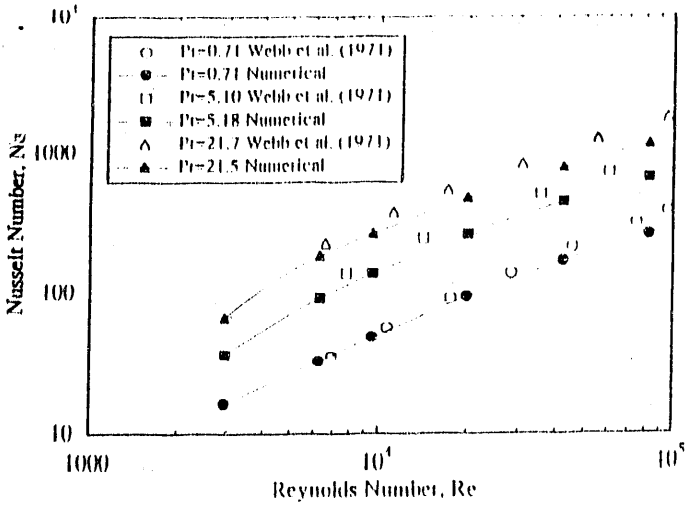


FIGURE 7 Comparison of the Predicted and Measured Mean Nusselt Numbers as a Function of the Reynolds Number

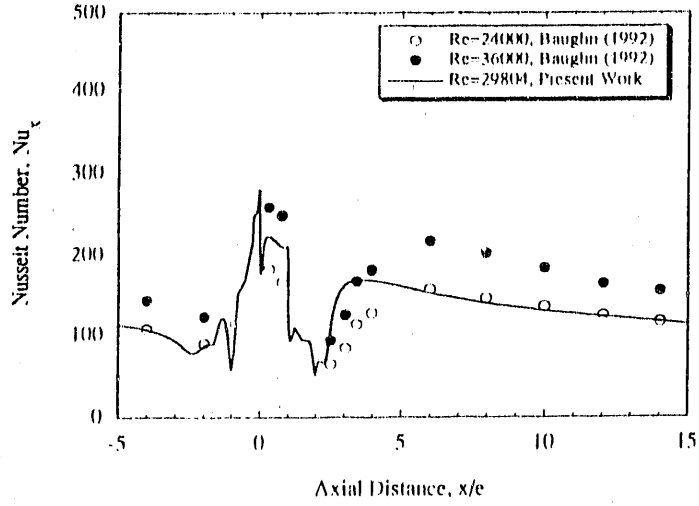


FIGURE 8 Comparison of the Predicted and Measured Local Nusselt Numbers as a Function of Axial Distance

Table 2 - Comparison Between the Measured and Predicted Nusselt Numbers for the Five Tubes Tested by Webb et al. (1971)

| Tube No. | Re | % Deviation | Re | % Deviation | Re | % Deviation | Re | % Deviation |
|---|---|---|---|---|---|---|---|---|
| 01/10 | 6113 | -13.71 | 6142 | 12.08 | 6122 | 12.36 | 6080 | 3.57 |
| | 9512 | 4.03 | 9506 | 18.28 | 9545 | 16.35 | 9537 | 9.77 |
| | 19860 | 19.66 | 20054 | 22.53 | 20021 | 21.48 | 20014 | 16.97 |
| | 42717 | 28.23 | 42905 | 27.10 | 42833 | 27.52 | 42684 | 15.80 |
| 02/10 | 6345 | 11.96 | 6383 | 22.10 | 6363 | 21.85 | 6321 | 17.55 |
| | 9761 | 13.83 | 9750 | 22.16 | 9789 | 18.60 | 9782 | 15.62 |
| | 20745 | 16.33 | 20833 | 17.58 | 20799 | 17.97 | 20316 | 14.65 |
| | 44645 | 24.93 | 44847 | 19.47 | 44615 | 24.24 | 44610 | 19.76 |
| 04/10 | 6465 | 7.51 | 6489 | 21.22 | 6469 | 23.86 | | |
| | 9497 | 6.31 | 9491 | 19.76 | 9533 | 23.15 | | |
| | 19156 | 8.81 | 19238 | 19.42 | 19207 | 25.17 | | |
| | 43157 | 18.94 | 43360 | 25.61 | 43282 | 31.23 | | |
| 02/20 | 6251 | .22 | 6287 | 18.70 | 6268 | 14.92 | | |
| | 9540 | 1.80 | 9530 | 18.32 | 9567 | 18.24 | | |
| | 19988 | 2.91 | 20067 | 20.09 | 20037 | 22.45 | | |
| | 42131 | 15.19 | 42313 | 22.71 | 42233 | 26.02 | | |
| | 82429 | 24.19 | 82436 | 26.02 | 82476 | 29.35 | | |
| 02/40 | 6319 | -13.73 | 6356 | 9.78 | 6336 | 1.61 | 7128 | 1.45 |
| | 9665 | 6.93 | 9655 | 11.65 | 9691 | 11.02 | 9968 | 13.17 |
| | 19599 | .68 | 19679 | 16.14 | 19639 | 19.19 | 19644 | 20.61 |
| | 39928 | 3.87 | 40093 | 16.95 | 40030 | 22.28 | 39899 | 18.01 |
| | 76605 | 8.67 | | | 76656 | 23.03 | | |

Average % Deviation = 15.35

agreement was also obtained between the measured and predicted friction factors (Arman and Rabas, 1992, 1991) for all five tubes tested by Webb et al. (1971).

An additional comparison is presented using the local heat-transfer data of Baughn and Rody (1992). Figure 8 compares these experimental results with numerical predictions using air as the test fluid (Pr = 0.71). Note the good agreement between the experimental and predicted results. These and other experimental results of Baughn and Yan (1992, 1991) and Berger and Hau (1979) have demonstrated that the most significant contributions to the heat-transfer performance with the separation and reattachment mechanism occur at the top surface of the rib and in the downstream recirculation zone. These two maximums are clearly displayed in Figure 8.

This numerical model will next be used to understand how the Prandtl number influences the thermal performance.

## INFLUENCE OF THE PRANDTL NUMBER

This section of the paper will explain how the Prandtl number affects the enhancement-level data in the manner shown in Figures 3 and 6. An important concept for this understanding is that there are six discrete regions or zones that must be considered:

1) upstream recirculation zone,
2,3,4) the rib upstream, top, and downstream faces,
5) the downstream recirculation zone, and
6) the boundary-layer development zone.

Lewis (1975a, 1975b) first proposed this multiple-region approach to correlate the performance of enhanced tubes with the separation and reattachment mechanism. However, this farsighted approach has not been further developed by subsequent researchers.

The most important finding of this study is that the Prandtl number has a dramatic impact on the thermal performance at the disruption or rib. Figures 9a and 9b show the normalized Nusselt number ratios, $Nu/Nu_D$, as a function of the axial location with five different Reynolds numbers for Pr values of 0.71 and 21.7, respectively. The performance at both rib sides is also shown by "opening up" or extending the x axis. The vertical lines are used to separate the flow field into the six different zones. The four lines at the rib region are located at each of the four corners. With the Pr increase from 0.71 to 21.7, note the following changes to the enhancement levels:

1) lower in the front recirculation zone for most of the Re range (zone 1),
2) substantially higher at the rib (zones 2, 3, and 4),
3) almost no change in the downstream recirculation zone (zone 5), and
4) lower in the boundary-layer development zone (zone 6) for most of the Re range.

This pattern was observed for all five tube geometries considered for this study and described in Table 1.

There are two other maximums that occur only when the

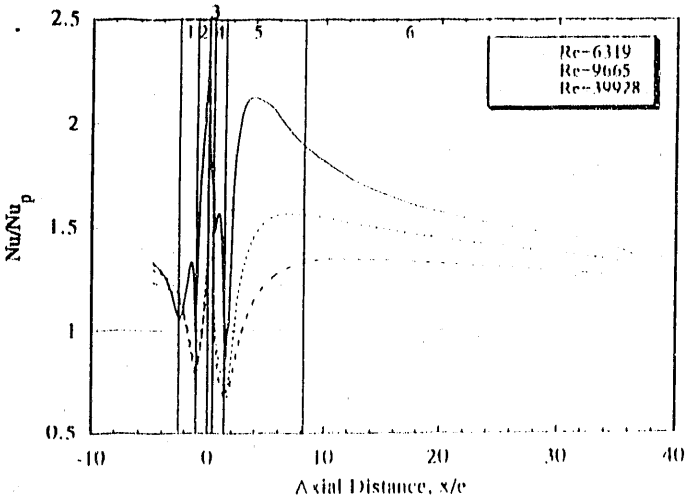


FIGURE 9a Local Nusselt Number Variation with Axial Distance for the 02/40 Tube with Pr = 0.71

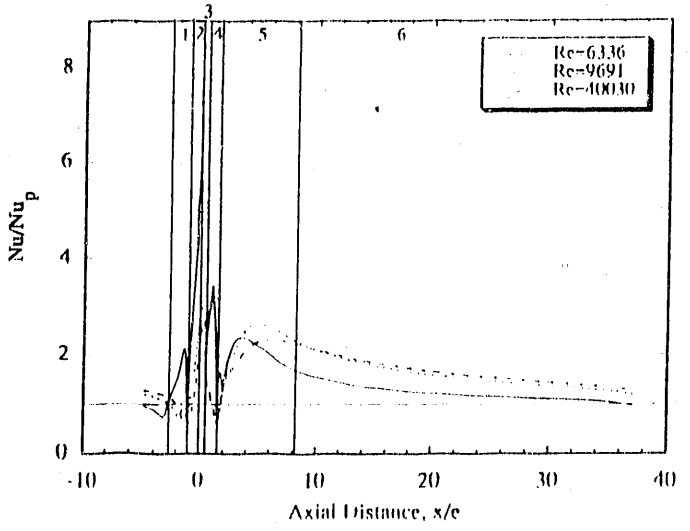


FIGURE 9b Local Nusselt Number Variation with Axial Distance for the 02/40 Tube with Pr = 21.7

Reynolds number, or more correctly the roughness Reynolds number or $e^+$, exceed a transition value that depends on the Prandtl number and the disruption geometry. Figure 9 shows these two other maximums in the rib area: one is located in the upstream separation region (zone 1), and the other is located on the vertical downstream face of the rib (zone 3). The authors are not aware of any experimental evidence that supports the existence of these additional maximums.

## Maximum Enhancement Level Variation at the Rib

Because the major Pr influence is concentrated at the rib, it was decided to determine the variation of the maximum enhancement level at this location in an attempt to explain Figures 3 and 6. Figure 10 shows the maximum values, $(Nu/Nu_p)_{max}$, at the rib as a function of the Reynolds number for Pr = 0.71 and 21.7 and for three tubes with the *p/e* value of 10. For air, the maximum enhancement levels increase to asymptotic values with increasing Reynolds number. For the higher Pr fluids, the maximum enhancement levels first increase, reach maximums, and then decrease. The Re value for the maximums depend on the $e/d_j$ value; the higher the $e/d_j$ value, the lower the Reynolds number required for the maximum. If the maximum enhancement-level data shown in

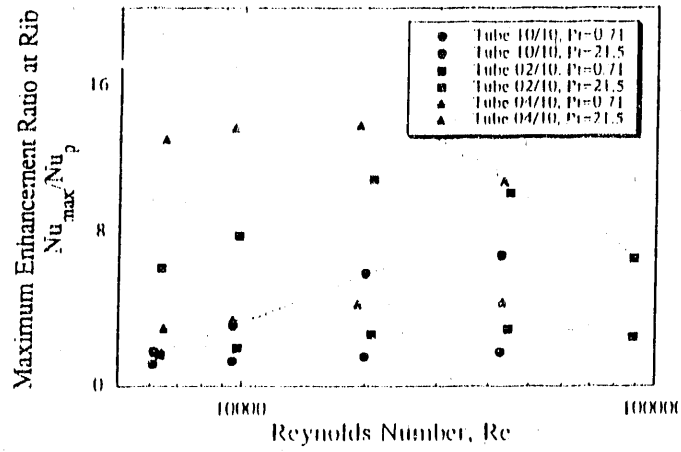


FIGURE 10 Maximum Enhancement Levels at the Rib for Pr = 0.71 and 21.7 and for the Three Tubes with a *p/e* Value of 10

Figure 10 were plotted with $e^+$ and for a single tube geometry, the influence of the Prandtl number on the shape of these curves would not be altered. But this variation is identical to that shown in Figures 3 and 6 for the mean enhancement-level variation with $e^+$. Another important finding is that the variations of the mean enhancement levels and the maximum enhancement levels at the rib follow identical patterns with changes of the Prandtl number and the roughness Reynolds number.

The actual mechanisms that are responsible for this enhancement-level variation with the Prandtl number at the rib region are very complicated and merit further investigation. In particular, the ability of the numerical model to capture the important flow details has not been demonstrated, although it was somewhat successful in predicting the local heat-transfer-coefficient variations for air. However, a possible explanation is as follows. The flow field at the three rib surfaces consists of separating and reattaching flows. For these flows, it has been established that the heat-transfer-coefficient dependence on the Reynolds number is in the 0.65 to 0.75 range. Some flow conditions that support this statement are cross flow to a single tube and impinging jet flows. Another example is the measured mean mass-transfer coefficients obtained with the naphthalene method (Pr = 2.5) for the three faces of a wall-mounted cube (Chyu and Natarajan, 1991). The exponents ranged from 0.626 to 0.661. For boundary-layer flows, Figures 4 and 5 show that the exponent on the Reynolds number is in the 0.65 to 0.75 range for air and in the 0.80 to 0.85 range for water and higher Prandtl number fluids.

Consider now the effect of an increasing flow rate on the enhancement level at the rib. It first increases with increasing Re or $e^+$ due to the turbulence caused by the rib penetration of the laminar sublayer. With a further increase, the separating and reattaching flow characteristics begin to dominate. For air, the enhancement level continues to increase and reach an asymptotic value because of the comparable exponents. However for higher Pr fluids, the enhancement level begins to decrease because the exponents for separting and reattaching flows are less than for boundary-layer flows.

## Influence of the Pitch on the Rib Thermal Performance

The maximum enhancement level at the rib decreases with an increase of the pitch or spacing of the disruptions; however, the magnitude of this decrease depends on the Prandtl number. Figure 11 shows the maximum enhancement levels as a function of the Reynolds number for two Prandtl number fluids and the 02/10, 02/20, and 02/40 tube geometries. Note the

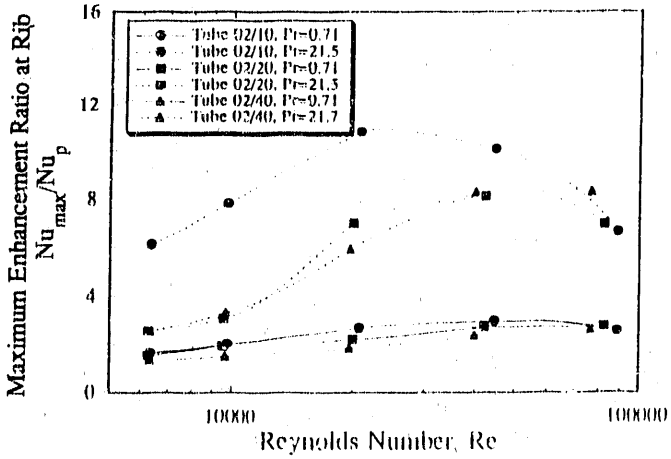


FIGURE 11 Maximum Enhancement Levels at the Rib for Pr = 0.71 and 21.7 and for the Three Tubes with $e/d_i$ Values of 0.02

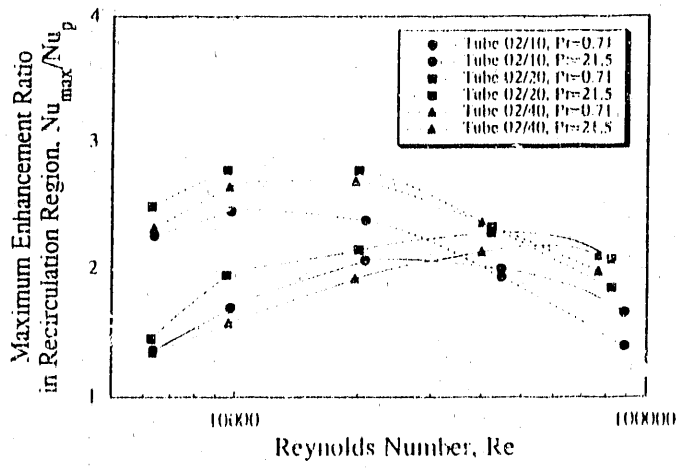


FIGURE 12 Maximum Heat-Transfer Enhancement in the Downstream Recirculation Region as a Function of the Reynolds Number for Pr = 0.71 and 21.7 and the Three Tubes with $e/d_i$ Value of 0.02

almost identical enhancement-level values for air but an increased departure for the larger Pr fluid. The explanation is that the impact of the upstream rib decreases with the separation or elongated boundary-layer development region. However, the sensitivity to the perturbations of the flow caused by the upstream rib increases with an increased Prandtl number.

For lower Pr fluids, the mean thermal performance is dependent on the pitch, although it has a small effect on the thermal performance at the rib. For air and, to a lesser extent, water, the contributions of the downstream recirculation zone and the boundary-layer development zones make a significant contribution to the mean thermal performance. The influence of the Prandtl number in the downstream recirculation zone is discussed next.

## Thermal Performance in the Downstream Recirculation Region

The second most important contribution to the total heat transfer comes from the downstream recirculation region, or zone 5. For low Pr fluids, this contribution is dominant as shown in Figure 9a. This section discussed the magnitude and location of the maximum heat transfer in the downstream recirculation region.

Figure 12 shows $(Nu/Nu_p)_{max}$ as a function of the Reynolds number for Pr = 0.71 and Pr = 21.7 and the 02/10, 02/20, and 02/40 tube geometries. For air (Pr = 0.71), the enhancement level increases with the Reynolds number; for Pr = 21.7, a definite maximum again exists as for the mean enhancement level and for the maximum enhancement level at the rib. This finding should not be a surprise. An extensive review of reattaching flows (Ota and Nishiyama, 1987) established that the maximum local-heat-transfer-coefficient dependency as expressed by the exponents on the Reynolds and Prandtl numbers are about 0.67 and 0.33, respectively. As a result, the influence of the Prandtl number on the thermal performance in the downstream recirculation zone is identical to that at the rib. The major finding of this investigation is that the mean thermal performance, as displayed by Figures 3 and 6, is the manifestation of the performance characteristics that occur at the two points of maximum heat transfer, at the rib and within the downstream recirculation zone.

Two possible reasons could account for the heat-transfer enhancement in the downstream recirculation zone:

1) The thickness of the thermal boundary layer decreases and the temperature gradient increases due to the flow impacting the surface near the reattachment point.
2) The temperature gradient is increased due to the high levels of turbulence near the surface.

Experimental evidence has been presented by Mori and Daikoku (1972) that demonstrates the latter is the correct reason. This point can be further substantiated with results from the numerical model. Figure 13 shows the turbulent-kinetic-energy variation in the radial direction at various locations downstream from the rib for the 02/20 tube geometry. Note the very high values of $k^+$ in the x/e = 2.6 and 5.3 range that is within the downstream recirculation zone. It will next be shown that the location of the maximum turbulent kinetic energy is near the location of the maximum heat transfer.

Comparisons of the locations of the maximum heat transfer, the maximum wall shear stress, the reattachment point, and the maximum turbulent kinetic energy are now presented. The locations of the maximum heat transfer in the recirculation region were obtained from plots similar to Figures 9a and 9b. The locations of the maximum wall shear stress and the reattachment points were obtained from plots of the wall shear stress similar to Figure 14. The wall shear stress is equal to zero at the reattachment point.

Figure 15 shows these characteristic lengths expressed as multiples of the rib height for the 02/20 tube geometry. Note the location of the maximum heat transfer 1) is between the reattachment-point location and the location of the maximum shear stress, 2) moves towards the upstream rib as the Reynolds number and Prandtl number are increased, and 3) is in the region of the maximum turbulent kinetic energy shown in Figure 13 (x/e in the 2.6 to 5.3 range). Previous experiment studies (Hijikata et al., 1987 and Hijikata and Mori, 1987) also suggested that the location of the maximum heat transfer is in front of the reattachment point and Berger and Hau (1979) discovered that the location moves forward with increasing Reynolds number. However, these studies did not investigate the influence of the Prandtl number on this location.

Figure 16 is a similar plot of the characteristic lengths for the 02/10 tube geometry. The common features of Figures 15 and 16 are the movement of the maximum heat-transfer locations towards the upstream rib with increasing Pr and Re

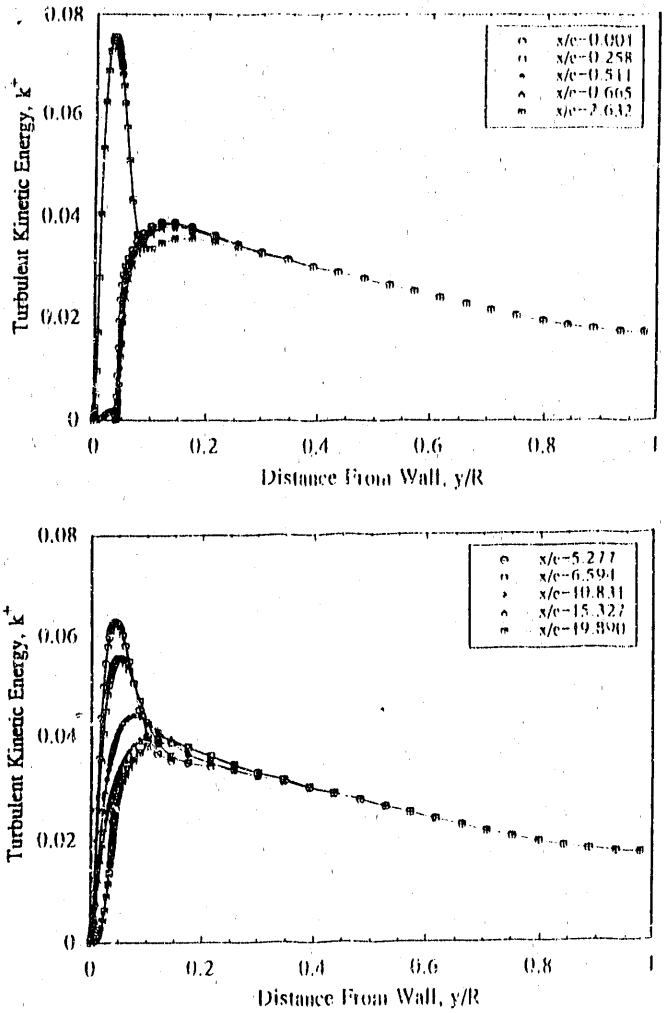


FIGURE 13 Turbulent Kinetic Energy Variation, $k^+$, with Distance from the Wall at Various Axial Locations, x/e for the 02/20 Tube Geometry

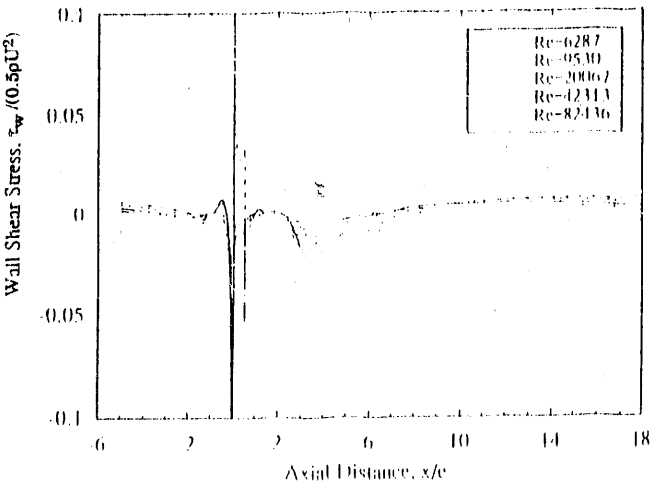


FIGURE 14 Local Wall Shear Stress as a Function of the Axial Location for the 02/20 Tube Geometry

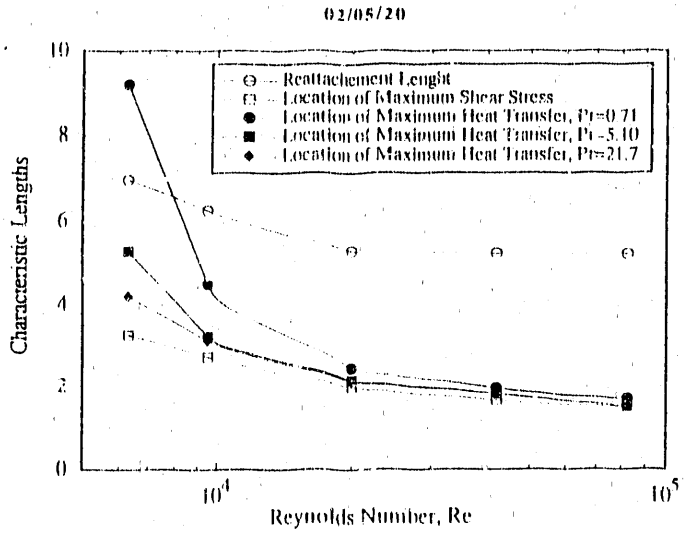


FIGURE 15 Characteristic lengths of the Downstream Recalculation Zone for the 02/20 Tube Geometry

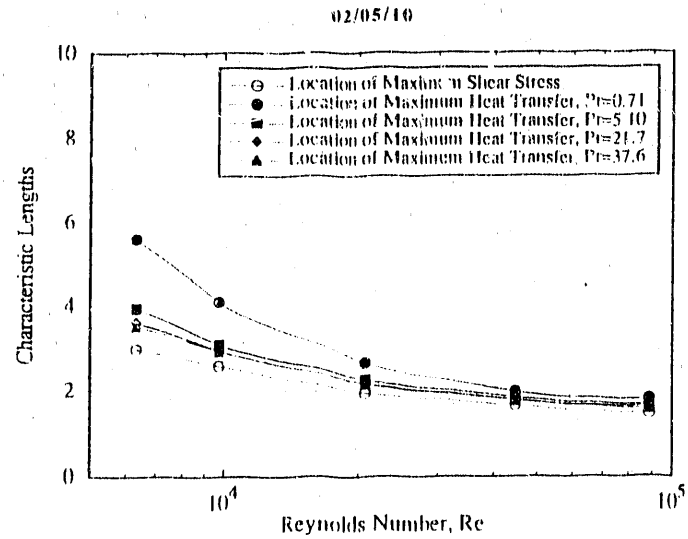


FIGURE 16 Characteristic lengths of the Downstream Recalculation Zone for the 02/10 Tube Geometry

and these locations being bounded from below by the locations of the maximum wall shear stress. For the tubes with $p/e = 10$, there were no reattachment points, or the local shear-stress values did not become positive after the rib. The authors were unable to find any experimental data to confirm or contradict this finding. The common belief was that the reattachment point always exists near the point of maximum heat transfer, even for $p/e$ values greater than about eight.

All the important findings regarding the influence of the Prandtl number on the thermal performance of enhanced tubes with the separation and reattachment mechanism are now summarized.

## CONCLUSIONS

Some fundamental findings about the influence of the Prandtl number on the thermal performance of enhanced tubes with the separation and reattachment mechanism are as follows:

1) Six distinct zones must be considered although some are far more important than others in their contributions to the heat-transfer performance.

2) Two major maximums in the thermal performance exist at the top surface of the rib and in the downstream recirculation zone in front of the reattachment point.

3) An increasing Prandtl number leads to a substantial increase of the heat-transfer enhancement at the rib. For high Pr fluids, the mean thermal performance is dominated by what happens at the rib.

4) The mean thermal performance exhibits the same variation as the maximum enhancement level at the rib when plotted as a function of the roughness Reynolds number, $e^+$.

5) The heat-transfer maximum in the downstream recirculation zone moves toward the rib with increasing Reynolds and Prandtl numbers. The location is between the reattachment point and the point of the maximum wall shear stress.

6) The influence of the Prandtl number on the thermal performance in the downstream recirculation zone is identical to that at the rib.

7) The cause of the heat-transfer improvement in the downstream recirculation zone is the high turbulence levels near the surface.

8) Two additional maximums occur at large roughness Reynolds numbers in the front recirculation zone and on the rear face of the rib.

9) The location of the reattachment point moves closer to the rib with increasing Reynolds number.

## REFERENCES


Arman, B. and T.J. Rabas, 1992a, Argonne National Laboratory Report, unpublished information.

Arman B., and T.J. Rabas, 1991, "Prediction of the Pressure Drop in Transverse, Repeated-Rib Tubes with Numerical Modeling," *Fouling and Enhancement Interactions*, ASME HTD-Vol. 164, pp. 93-99.

Baughn, J.W. and J. Rody, 1992, "Enhanced Turbulent Heat Transfer in Circular Ducts with Transverse Ribs," paper to be presented at the National Heat Transfer Conference, San Diego, August 9-12, 1992.

Baughn, J.W. and X. Yan, 1992, "Local Heat Transfer Measurements in Square Ducts, with Transverse and Diagonal Ribs," paper to be presented at the National Heat Transfer Conference, San Diego, August 9-12, 1992.

Baughn, J.W. and X. Yan, 1991, "An Insertion Technique Using the Transient Method with Liquid Crystals for Heat Transfer Measurements in Ducts," *Fouling and Enhancement Interactions*, ASME, HTD-Vol. 164, pp. 77-84.

Berger, F.P., and K. F., F.-L. Hau, 1979, "Local Mass/Heat Transfer Distribution on Surfaces Roughened with Small Square Ribs," *International Journal of Heat and Mass Transfer*, Vol. 22, pp. 1645-1656.

Burck, E., 1970, "The Influence of Prandtl Number on Heat Transfer and Pressure Drop of Artificially Roughened Channels," *Augmentation of Convective Heat and Mass Transfer*, ASME Symposium Volume, pp. 27-35.

Carnavos, T.C., 1980, "Heat Transfer Performance of Internally Finned Tubes in Turbulent Flow," *Heat Transfer Engineering*, Vol. 1, No. 4, pp. 32-37.

Carnavos, T.C. 1979, "Cooling Air in Turbulent Flow with Internally Finned Tubes," *Heat Transfer Engineering*, Vol. 1, No. 2, pp. 41-46.

Chen, H.C., and V.C. Patel, 1988, "Near-Wall Turbulence Models for Complex Flows Including Separation," *AIAA Journal.*, Vol 26, pp. 641-648.

Chyu, M.K. and V. Natarajan, 1991, "Local Heat/Mass Transfer Distributions on the Surfaces of a Wall Mounted Cube," *ASME Journal of Heat Transfer*, Vol. 113, pp. 851-857.

Dawson, D.A., and O. Trass, 1972, "Mass Transfer at Rough Surfaces," *International Journal of Heat and Mass Transfer*, Vol. 15, pp. 1317-1336.

Dipprey, D.F., and R.H. Sabersky, 1963, "Heat and Momentum Transfer in Smooth and Rough Tubes at Various Prandtl Numbers," *International Journal of Heat and Mass Transfer*, Vol. 6, pp. 329-353.

Gowen, R.A., and J.W. Smith, 1968, "Turbulent Heat Transfer from Smooth and Rough Surfaces," *International Journal of Heat and Mass Transfer*, Vol. 11, pp. 1657-1673.

Hijikata, K., H. Ishiguro, and Y. Mori, 1987, "Heat Transfer Augmentation in a Pipe Flow with Smooth Cascade Turbulence Promoters and Its Application to Energy Conversion," *Heat Transfer in High Technology and Power Engineering*, Eds. W.J. Yang and Y. Mori, Hemisphere Publishing Corp., Washington, D.C., pp. 368-379.

Hijikata, K., and Y. Mori, 1987, "Fundamental Study of Heat Transfer Augmentation of Tube Inside Surface by Cascade Smooth Surface-Turbulence Promotors," *Wärme und Stoffübertragung*, Vol. 21, pp. 115-124.

Kalinin, E.K., G.A. Drietser, S.A. Yarkho, and V.A. Kusminov, 1970, "The Experimental Study of the Heat Transfer Intensification Under Conditions of Forced One- and Two-Phase Flow in Channels," *Augmentation of Convective Heat and Mass Transfer*, ASME Symposium Volume, pp. 89-90.

Leonard, B.P., 1979, "A Stable and Accurate Corrective Modeling Procedure Based on Quadratic-Upstream Interpolation," *Computer Methods in Applied Mechanics and Engineering*, Vol. 19, pp 59-98.

Lewis, M.J., 1975a "An Elementary Analysis for Predicting the Momentum- and Heat-Transfer Characteristics of Hydraulically Rough Surfaces," *ASME Journal of Heat Transfer*, Vol. 97, pp. 249-254.

Lewis, M.J., 1975b, "Optimizing the Thermohydraulic Performance of Rough Surfaces," *International Journal of Heat and Mass Transfer*, Vol. 18, pp. 1243-1248.

Mendes, P.R.S., and M.H.P. Mauricio, 1987, "Heat Transfer, Pressure Drop, and Enhancement Characteristics of the Turbulent Through Internally Ribbed Tubes," *Convective Transport*, ASME HTD-Vol. 82, pp. 15-22.

Mori, Y. and T. Daikoku, 1972, "Effect of 2-Dimensional Roughness on Forced Convective Heat Transfer," *Bulletin of JSME*, Vol. 15, No. 90, pp. 1581-1590.

Ota, T. and H. Nishiyama, 1987, "A Correlation of Maximum Turbulent Heat Transfer Coefficient on Reattachment Flow Region," *International Journal of Heat and Mass Transfer*, Vol. 30, No. 6, pp. 1193-1200.

Patankar, S.V., 1980, "Numerical Heat Transfer and Fluid Flows," McGraw-Hill, New York.

Patankar, S.V., C.H. Liu, and E.M. Sparrow, 1977, "Fully Developed Flow and Heat Transfer in Ducts Having Streamwise Periodic Variations of Cross-Sectional Area," *ASME Journal of Heat Transfer*, Vol. 99, pp. 180-186.

Patankar S., and D.B. Spalding, 1972, "A Calculation Procedure for Heat, Mass and Momentum Transfer in Three-Dimensional Parabolic Flows," *International Journal of Heat and Mass Transfer*, Vol. 15, pp. 1887-1906.

Petukov, B.S., 1970, "Heat Transfer and Friction Factor in Turbulent Pipe Flow with Variable Physical Properties," *Advances in Heat Transfer*, Vol. 6, pp. 503-564.

Phillips, R.E., and F.W. Schmidt, 1985, "Multigrid Techniques for the Solution of Passive Scalar Advection-Diffusion Equation," *Numerical Heat Transfer*, Vol. 8, pp. 25-43.

Rabas, T.J., 1989, "Selection of the Energy-Efficient Enhancement Geometry for Single-Phase Turbulent Flow Inside Tubes," *Heat Transfer Equipment Fundamentals, Design, Applications and Operating Problems*, ASME HTD-Vol. 108, pp. 193-204.

Savage, D.W., and J.E. Myers, 1963, "The Effect of Artificial Surface Roughness on Heat and Momentum Transfer," *AIChE Journal*, Vol. 9, pp. 694-702.

Smith, J.W., and R.A. Gowen, 1965, "Heat Transfer Efficiency in Rough Pipes at High Prandtl Number," *AIChE Journal*, Vol. 11, pp. 941-943.

Tan, Y.K., and J.W. Xiao, 1989, "Influence of Prandtl Number to Fluid Heat Transfer Characteristics of Spirally Corrugated Tubes," *The Fourth Asian Congress of Fluid Mechanics*, Hong Kong

Van Doormal, J.P., and G.D. Raithby, 1984, "Enhancements of the SIMPLE Method for Predicting Incompressible Fluid Flows," *Numerical Heat Transfer*, Vol. 7, pp. 147-163.

Webb, R.L., 1979, "Toward a Common Understanding of the Performance and Selection of Roughness for Forced Convection," *Studies in Heat Transfer, A Festschrift for E.R.G. Eckert*, ed. J.P. Hartnett, Hemisphere, Washington, pp. 252-272.

Webb, R.L., E.R.G. Eckert, and R.J. Goldstein, 1971, "Heat Transfer and Friction in Tubes with Repeated-Rib Roughness," *International Journal of Heat and Mass Transfer*, Vol. 14, pp. 601-617

## APPENDIX

This appendix explains the method used to make the comparison of the efficiency-index values predicted by the correlation of Burck (1970) with the experimental data of Webb et al. (1971).

The correlation proposed by Burck is as follows

$$\eta = 1.25 - 0.32\times10^{-3}\log(e_{sg}^{+}) + \log(Pr^{0.33}e_{sg}^{+0.213})$$

In order to calculate the efficiency index, the sand-grain roughness Reynolds number, $e_{sg}^{+}$, is required. This quantity is obtained with the following calculation procedure. The first step is to calculate the sand-grain roughness using the fully rough friction-factor equation

$$f = 1/[2\log(d_i/e_{sg}) + 1.74]^2$$

The measured friction-factor values for all of the tube geometries tested by Webb et al. (1971) were used to calculate the $d_i/e_{sg}$ with the above equation using a trial-and-error procedure. Next, the sand-grain roughness Reynolds number was calculated, or $e_{sg}^{+} = (e_{sg}/d_i)Re\sqrt{f/2}$.

Table 3 compares the efficiency-index values obtained with the above method, $\eta_{Burck}$, with the values obtained from the experimental data of Webb et al. (1971), $\eta_{Exp}$. Note that substantial errors exist, for some cases by almost a factor of two.

Table 3 - Comparison of the Experimental (Webb et al., 1971) and Predicted (Burck, 1970) Efficiency Index Values

| Pr | Re | f | $e_{sg}/D$ | $e_{sg}^{+}$ | $\eta_{Burck}$ | $\eta_{Exp}$ |
|---|---|---|---|---|---|---|
| | | | **Tube 01/10** | | | |
| 71 | 6000 | 0130 | 01282 | 20 71 | 882 | 638 |
| 71 | 10000 | 0161 | 07938 | 71 22 | 754 | 585 |
| 71 | 30000 | 0202 | 12912 | 519 07 | 565 | 524 |
| 5 10 | 6000 | 0130 | 01282 | 20 71 | 1 159 | 811 |
| 5 10 | 10000 | 0161 | 07938 | 71 22 | 1 017 | 843 |
| 5 10 | 30000 | 0202 | 12912 | 519 07 | 706 | 625 |
| 21 70 | 6000 | 0130 | 01282 | 20 71 | 1 362 | 1 018 |
| 21 70 | 10000 | 0161 | 07938 | 71 22 | 1 210 | 1 109 |
| 21 70 | 30000 | 0202 | 12912 | 519 07 | 809 | 747 |
| 37 60 | 6000 | 0130 | 01282 | 20 71 | 1 439 | 1 000 |
| 37 60 | 10000 | 0161 | 07938 | 71 22 | 1 286 | 1 223 |
| 37 60 | 30000 | 0202 | 12912 | 519 07 | 848 | 724 |
| | | | **Tube 02/10** | | | |
| 71 | 6000 | 0250 | 19147 | 130 46 | 693 | 520 |
| 71 | 10000 | 0302 | 27003 | 331 82 | 601 | 471 |
| 71 | 30000 | 0354 | 37775 | 1650 68 | 495 | 364 |
| 5 10 | 6000 | 0250 | 19147 | 130 46 | 939 | 893 |
| 5 10 | 10000 | 0302 | 27003 | 331 82 | 795 | 687 |
| 21 70 | 6000 | 0250 | 19147 | 130 46 | 1 121 | 1 065 |
| 21 70 | 10000 | 0302 | 27003 | 331 82 | 936 | 787 |
| 37 60 | 6000 | 0250 | 19147 | 130 46 | 1 190 | 1 128 |
| 37 60 | 10000 | 0302 | 27003 | 331 82 | 980 | 828 |
| | | | **Tube 02/20** | | | |
| 71 | 6000 | 0186 | 10887 | 62 99 | 766 | 609 |
| 71 | 10000 | 0202 | 12912 | 129 77 | 693 | 597 |
| 71 | 30000 | 0259 | 20729 | 913 56 | 523 | 423 |
| 5 10 | 6000 | 0186 | 10887 | 62 99 | 1 032 | 1 016 |
| 5 10 | 10000 | 0202 | 12912 | 129 77 | 910 | 868 |
| 5 10 | 30000 | 0259 | 20729 | 913 56 | 512 | 475 |
| 21 70 | 6000 | 0186 | 10887 | 62 99 | 1 226 | 1 215 |
| 21 70 | 10000 | 0202 | 12912 | 129 77 | 1 122 | 951 |
| | | | **Tube 02/40** | | | |
| 71 | 6000 | 0141 | 01653 | 23 41 | 869 | 605 |
| 71 | 10000 | 0151 | 01451 | 38 67 | 817 | 618 |
| 71 | 30000 | 0165 | 08390 | 303 82 | 611 | 521 |
| 71 | 100000 | 0172 | 09200 | 853 13 | 529 | 422 |
| 5 10 | 6000 | 0141 | 01653 | 23 41 | 1 115 | 1 019 |
| 5 10 | 10000 | 0151 | 01451 | 38 67 | 1 089 | 928 |
| 5 10 | 30000 | 0165 | 08390 | 303 82 | 810 | 615 |
| 21 70 | 6000 | 0141 | 01653 | 23 41 | 1 318 | 1 188 |
| 21 70 | 10000 | 0151 | 01451 | 38 67 | 1 288 | 1 032 |
| 21 70 | 30000 | 0165 | 08390 | 303 82 | 957 | 668 |
| 37 60 | 6000 | 0141 | 01653 | 23 41 | 1 425 | 1 280 |
| 37 60 | 10000 | 0151 | 01451 | 38 67 | 1 361 | 1 111 |
| 37 60 | 30000 | 0165 | 08390 | 303 82 | 1 012 | 654 |
| | | | **Tube 04/10** | | | |
| 71 | 6000 | 0592 | 69581 | 218 30 | 541 | 306 |
| 71 | 10000 | 0537 | 70278 | 1211 20 | 509 | 286 |
| 5 10 | 6000 | 0592 | 69581 | 218 30 | 626 | 365 |
| 5 10 | 10000 | 0537 | 70278 | 1211 20 | 450 | 309 |
| 21 70 | 6000 | 0592 | 69564 | 218 30 | 689 | 521 |

# END

# DATE FILMED

9/4/92